CHINESE OPTICS LETTERS

Vol. 21, No. 6 | June 2023

Effects of laser waveform on the generation of fast electrons in laser–solid interactions

Xiaomei Dong (董晓梅)[1,2], Yuhan Du (杜昱晗)[2], Miaohua Xu (徐妙华)[2*], Yutong Li (李玉同)[3,4], Zhe Zhang (张 喆)[3,4**], and Yingjun Li (李英骏)[1***]

[1] State Key Laboratory for GeoMechanics and Deep Underground Engineering, China University of Mining and Technology (Beijing), Beijing 100083, China

[2] School of Science, China University of Mining and Technology (Beijing), Beijing 100089, China

[3] Institute Key Laboratory of Optic Physics, Institute of Physics, Chinese Academy of Sciences, Beijing 100190, China

[4] Songshan Lake Materials Laboratory, Dongguan 523808, China

*Corresponding author: mhxu@cumtb.edu.cn

**Corresponding author: zzhang@iphy.ac.cn

***Corresponding author: lyj@aphy.iphy.ac.cn

Received February 9, 2023 | Accepted March 24, 2023 | Posted Online June 6, 2023

In the scheme of fast ignition of inertial confinement fusion, the fuel temperature mainly relies on fast electrons, which act as an energy carrier, transferring the laser energy to the fuel. Both conversion efficiency from the laser to the fast electron and the energy spectrum of the fast electron are essentially important to achieve highly effective heating. In this study, a two-dimensional particle in cell simulation is applied to study the generation of fast electrons from solid-density plasmas with different laser waveforms. The results have shown that the slope of the rising edge has a significant effect on fast electron generation and energy absorption. For the negative skew pulse with a relatively slow rising edge, the $J \times B$ mechanism can most effectively accelerate the electrons. The overall absorption efficiency of the laser energy is optimized, and the fast electron yield in the middle- and low-energy range is also improved.

Keywords: laser waveform; fast electrons; particle-in-cell simulations; plasmas.
DOI: 10.3788/COL202321.063801

1. Introduction

In inertial confinement fusion (ICF) schemes such as fast ignition[1] and double cone ignition[2], first high-energy nanosecond laser beams are used to compress the target into a high-density plasma (with density approaching 100 g/cm^3). Then the fast electron beam generated by the high-power petawatt laser quickly heats the precompressed fuel in a short period of time. In order to obtain better heating effect, higher laser energy and higher heating efficiency are needed. It is very costly and difficult to further promote laser energy due to the limitations on high-power laser devices and optics, especially the large aperture gratings. Under such conditions, it is particularly important to improve the heating efficiency of fast electrons. Under the typical compression state in fast ignition, the penetration depth of fast electrons with energy of 0.5–2 MeV is similar to that of alpha particles and has a higher heating efficiency. The electrons of lower energy cannot penetrate through the high-density plasma, while electrons with higher energy penetrate through the dense core region with residual kinetic energy, both leading to reduced heating efficiency. Johzaki *et al.* have used the Fokker–Planck simulation program to reproduce this physical process by simulating the heating of the core pellet by fast electrons guided by a conical target[3,4]. Therefore, for the heating stage, the fast electron yield in the range of 0.5–2 MeV is more important.

Theoretical and experimental research has been carried out to study the properties of fast electrons generated in the interaction between laser and solid-density plasma (including the yield, energy distribution, angular distribution, etc.). Studies have shown that the generation of fast electrons is closely related to the target and laser parameters. For the target, researchers have studied the material, thickness, geometry, and preplasma in detail and have proposed optimization schemes[5–8]. The results have shown that a conical structure has the advantage of effectively guiding the laser and the electrons and has become the preferred choice for fast ignition[9]. The coupling efficiency of laser energy can be further improved and the fast electron divergence angle can be optimized by an external magnetic field[10]. For laser parameters, theoretical and experimental studies have mainly focused on the influence of laser energy, intensity, pulse width, and polarization[11–15].

Besides the parameters described above, the laser waveform is one of the important parameters affecting the interaction between laser and solid-density plasma. Theoretical and experimental results have shown that the waveform, the rising edge, and the asymmetry of the laser pulse have an influence on the wake field electron acceleration[16–19], the generation of terahertz radiation[20], and electron acceleration from vacuum[21]. With the development of laser technology, including the pulse-shaping technology such as programmable spatial light modulators, acousto-optic modulators, moving mirrors, deformable mirrors, and plasma optics, it is now possible to achieve asymmetric laser waveforms in experiments[22–26]. These technologies have provided the possibility studying the generation of fast electrons from asymmetric laser pulses. In this paper, we use the two-dimensional PIC code EPOCH[27] to simulate the fast electrons generated by laser pulses with different waveforms (including positive, Gaussian, and negative skew pulses). The simulation results show that the asymmetric laser pulse waveform can affect the generation of fast electrons and the energy absorption while the laser energy and the peak intensity are kept the same. The J × B mechanism works most efficiently in the case of negative skew pulses (with slow rising edges). The absorption efficiency of laser energy and the yield of fast electrons in the medium- and low-energy range have also been efficiently improved.

2. Simulation Conditions

In this paper, simulations of laser–plasma interaction are performed with varying laser temporal profile as well as constant laser energy and peak power. The effects of laser waveforms on fast electron generation are investigated. The p-polarized laser with wavelength $\lambda = 1.05$ μm irradiates the target at normal incidence, and its spatial beam profile in the y direction is uniform. The laser temporal profiles are shown in Fig. 1(a), where shape-1 is a positive skew pulse with a 50 fs rise time and a 750 fs fall time, shape-2 is a Gaussian pulse with a full width at half-maximum of 320 fs, and shape-3 is a negative skew pulse with a 750 fs rise time and a 50 fs fall time. For most of the laser facilities, the limitation of picosecond laser output is power damage threshold, so in our simulations, the peak intensity was kept constant as 1.5×10^{19} W/cm^2. The size of the simulation box is 170 μm × 16 μm with a grid size of $\lambda/64$. The whole simulation box contains 10880 × 1024 grid elements, and 20 particles are placed in each grid element. The thickness of the target was intentionally set as 120 μm in order to avoid the influence of the return current from the target rear surface and from the right boundary of the simulation box when we count the accelerated electrons. The initial density was set to $20n_c$ (n_c is the critical plasma density, expressed as $n_c = mw^2/4\pi e^2$, where m is the electron mass, w is the laser frequency, and e is the electron charge)[28], the ionization degree was 40, and the initial temperature was 1 keV. Boundary conditions in the x direction are open for particles and electromagnetic waves. In the y direction, periodic boundary conditions are applied for both particles and electromagnetic waves.

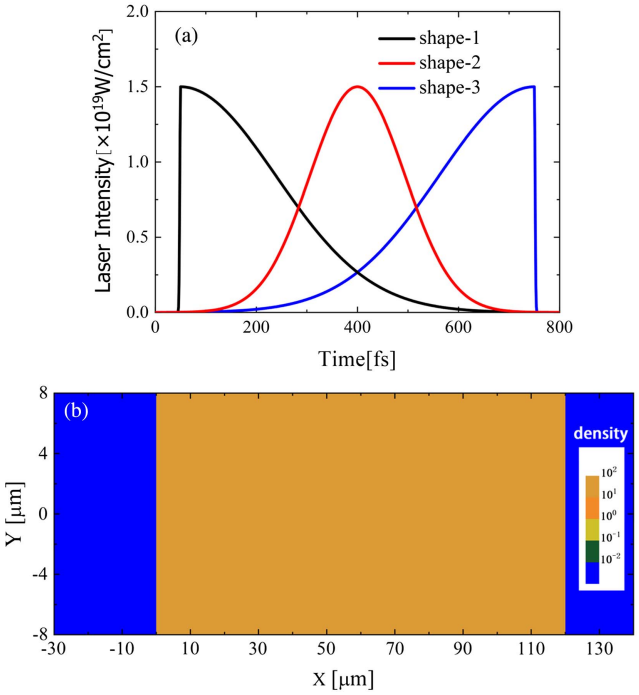

Fig. 1. (a) Laser temporal profiles in three simulated cases; (b) two-dimensional profile of electron density of the target plasma.

3. Results and Analysis

Time-integrated energy spectra of fast electrons for the three cases are shown in Fig. 2. A region with a thickness of 1 μm at the position of $X = 5$ μm was selected for electron counting, with 25 fs intervals. The inset of Fig. 2 shows the energy spectra

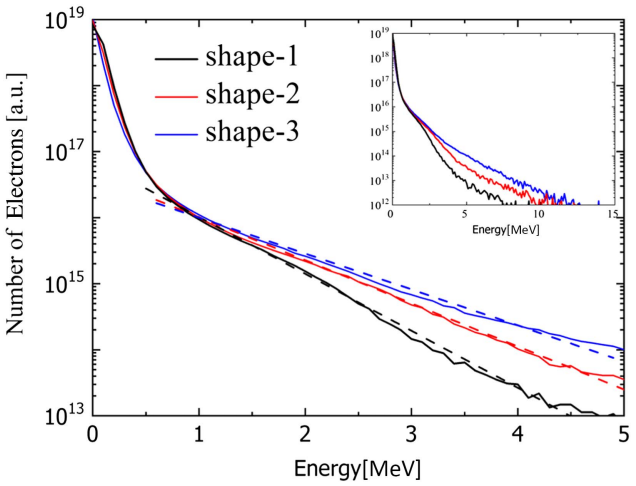

Fig. 2. Time-integrated energy spectra of fast electrons with three laser waveforms (a dashed line is utilized to indicate the temperature slope). The black line indicates the positive skew case. The red line indicates the Gaussian case. The blue line indicates the negative skew case.

of fast electrons in the range of 0–15 MeV. It may be seen that the fast electron yield with energy >0.5 MeV under the negative skew case is significantly higher than the other two cases. Second, the slope temperatures of the electrons are compared. For a positive skew pulse (with steep rising edges), the slope temperature of the electrons (> 0.5 MeV) is about 0.86 MeV, while the temperatures are 1.0 and 1.2 MeV for the Gaussian pulse (symmetric waveforms) and the negative skew pulse (with slow rising edges), respectively.

The electron intensities in different energy ranges, 0–0.5 MeV, 0.5–2 MeV, 2–5 MeV, and > 5 MeV, are investigated and compared for the three pulses. The results shows that the number of electrons at 0.5–2 MeV in the negative skew case is 9.0% larger than that in the Gaussian case, and 19.5% larger than that in the positive skew case. The electron amount in the energy range of 2–5 MeV exceeds in the Gaussian and positive skew cases by 41.9% and 217.4%, respectively.

When the ultra-intense laser pulse interacts with plasma, the laser energy can be absorbed by electrons through vacuum heating[29], resonance absorption[30], and the J × B mechanism[31,32]. Figure 3 shows the electron momentum (normalized to $m_e c$) distribution in phase space (X, P_X) in three simulated cases. It can be clearly seen that the electron beam with an interval of half a laser wavelength propagates into the target, which is consistent with the characteristics of the J × B mechanism, indicating that the J × B mechanism is the dominant acceleration mechanism under the current simulation parameters.

Figure 4 shows the spatial distribution of longitudinal momentum when the laser peak arrives at the target surface, which is 150 fs for the positive skew pulses, 500 fs for the Gaussian pulses, and 850 fs for the negative skew pulses. When the laser peak reaches the target surface, the maximum longitudinal momentum of the electrons at the front surface driven by the pondermotive force can reach $40m_e c$ for the negative skew pulse, while it is only $8m_e c$ for the positive pulse, although the peak laser intensity is exactly the same.

Figure 5 shows the time evolution of the maximum longitudinal momentum of the electrons around the target surface (in the region of $-1\,\mu\text{m} < X < 1\,\mu\text{m}$) for the three pulses. The laser waveforms are included, respectively, in the figure. It can be seen that for the positive skew waveforms with steep rising edges, the peak of the longitudinal momentum appears behind the laser peak significantly. For Gaussian waveforms, the delay time is shortened. For the negative skew pulses with slow rising edges, the peak of the longitudinal momentum almost coincides with the laser peak time. For the positive skew pulse, the electrons were not effectively accelerated when the laser peak interacted with the target surface, while in the case of the negative skew pulse, the electrons were most effectively accelerated. The maximum longitudinal momentum of the electrons accelerated by the negative skew pulses is significantly higher than those in the positive and Gaussian pulse shapes.

Although the peak intensity and laser energy of the three laser waveforms are the same, there are obvious differences in accelerated fast electrons. The main reason is the fact that the plasma conditions caused by the different rising edges of the three pulses differ. Figure 6 shows the plasma density distribution when the laser peak reaches the target surface under three laser waveforms.

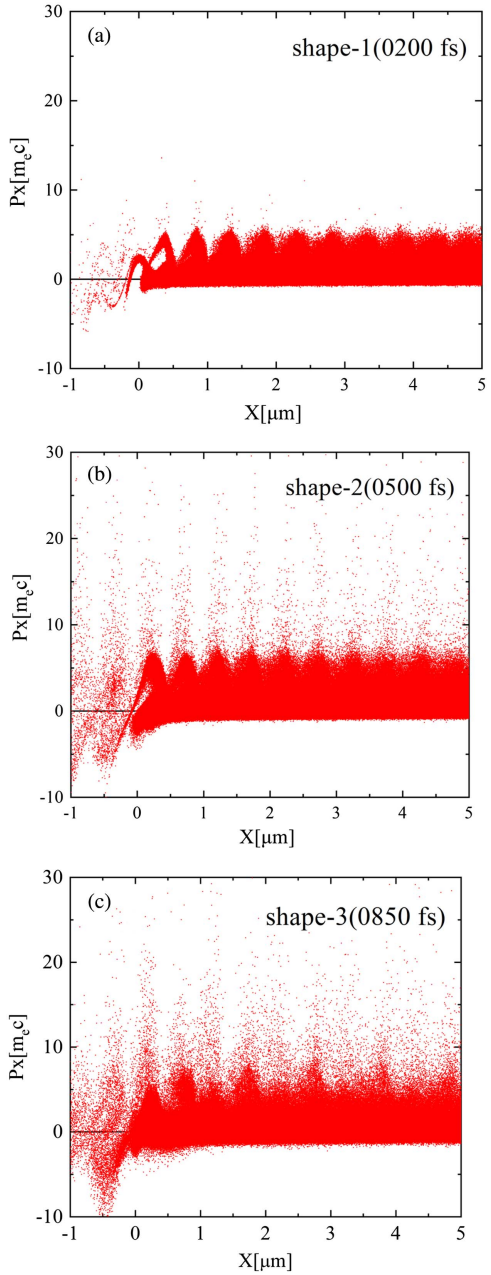

Fig. 3. Phase space (X, P_X) distribution of the electrons. (a) Positive skew pulses, 200 fs; (b) Gaussian pulses, 500 fs; (c) negative skew pulses, 850 fs.

As can be seen from Fig. 6, the scale length of the plasma is close to 0 when the laser peak reaches the target surface for positive skew pulse due to the very steep rising edges. The plasma has no time to expand before the laser peak arrives. At the same time, the steepening of the density profile is attributed to the ponderomotive force, leading to an increase in plasma density at the front surface, surpassing the initial density. Since the strength of the electrostatic field is proportional to the plasma density and is inversely proportional to the density scale length,

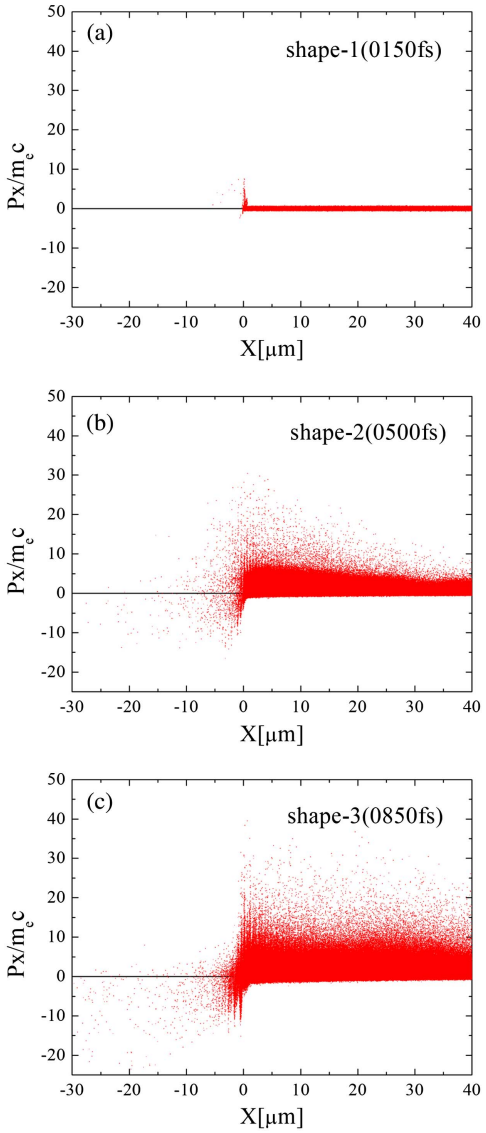

Fig. 4. Distribution of electrons' longitudinal momentum when the laser peak reaches the target surface. (a) Positive skew pulses, 150 fs; (b) Gaussian pulses, 500 fs; (c) negative skew pulses, 850 fs.

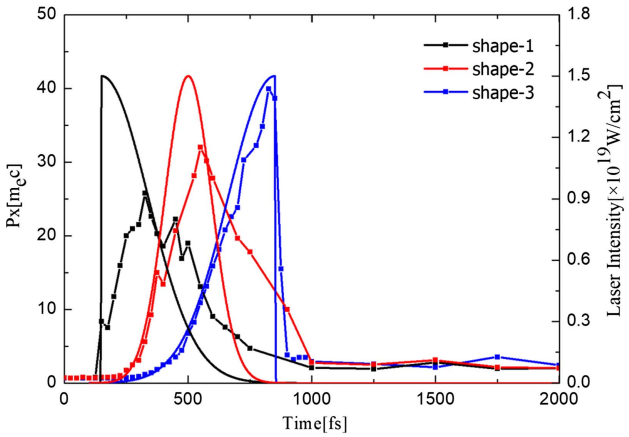

Fig. 5. Evolution of the maximum longitudinal momentum at the target surface for different laser waveforms. The black square line indicates the positive skew case. The red square line indicates the Gaussian case. The blue square line indicates the negative skew case.

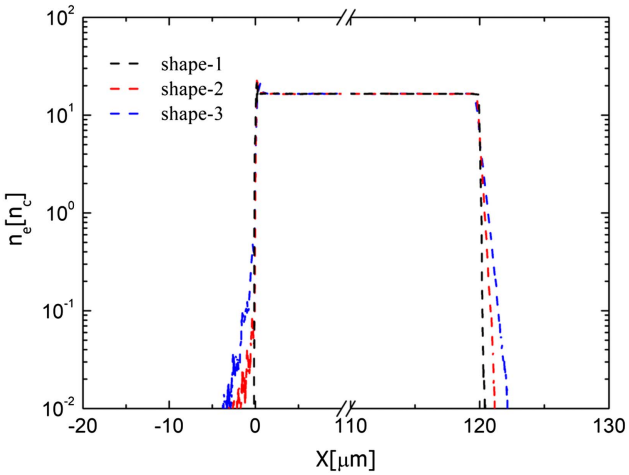

Fig. 6. Distribution of plasma density along the *x* direction when the laser peak reaches the front surface of the target for the different laser waveforms.

the electrostatic field thus has a more serious deceleration effect on the electrons. This is the main reason why the positive skew pulses cannot effectively accelerate the fast electrons at the peak time. After the peak intensity has passed, the plasma gradually expands, and the effect of the separation field becomes weak. However, the laser intensity has dropped, and the electrons cannot gain energy effectively from the laser at the later time as well. For the negative skew pulse, the plasma has expanded before the laser peak is reached, the influence of the electrostatic separation field is relatively weak, and the electrons on the front surface of the target can obtain more kinetic energy. As a result, the temperature of the fast electrons generated by the negative skew pulse is higher. Extensive theoretical and experimental studies[33–35] have also shown that the preplasma and its density scale length play a significant role in the fast electron generation in the J × B mechanism.

As shown in Figs. 7(a)–7(c), the time evolution of the energy absorbed by electrons from the laser has been further investigated. The total energy of electrons in the simulation box and with different energy ranges is illustrated. In Figs. 7(d)–7(f), the time evolutions of electron energy under three kinds of pulses are compared. It can be seen that the total energy of fast electrons with energies more than 500 keV, 1 MeV, and 5 MeV for negative skew pulses is significantly higher than that of the other two pulses, and the energy absorption efficiency of the laser is higher. In addition, it was found that the peaks of electron energy appear at about 400, 625, and 850 fs for positive, Gaussian and negative skew pulses. Compared with the laser peak, the peak time of electron energy in the three waveforms is delayed by 250, 125, and 0 fs. The energy absorption of the electrons in the case of the positive skew pulse is obviously

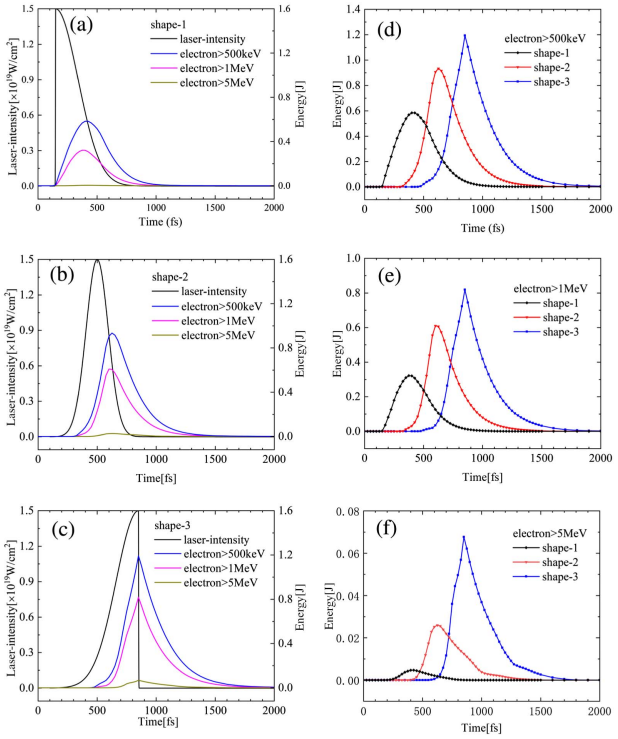

Fig. 7. Time evolution of the total energy of electrons in the simulation box with different energy ranges for the three pulses. (a) For positive skew pulses; (b) for Gaussian pulses; (c) for negative skew pulses. Comparison of the energy of electrons under the three pulses. (d) For electrons with $E >$ 500 keV; (e) for electrons with $E > 1$ MeV; (f) for electrons with $E > 5$ MeV.

lagging behind the energy input of the laser, while the energy absorption of the electrons for the negative skew pulse is basically consistent with the input of the laser energy.

Since the J × B mechanism depends on the magnetic field of the laser, the plasma region before the laser reflection is the region where the J × B mechanism can work effectively. Due to the short rising time of the positive skew pulse, the peak value reaches the target surface too early, and the high-density plasma at the front surface strongly reflects the laser. In this way, the region where the J × B mechanism can work is very thin, which results in a low absorption efficiency of laser energy. In time, although the plasma continues to expands and the thickness of the absorption area continues to increase, the laser energy decreases significantly. For the negative skew pulse, when the laser peak arrives at the front surface, the thickness of the absorption area is significantly larger than that of the positive skew pulse. In this way, more electrons can be driven by the laser ponderomotive force to obtain energy, leading to more absorption and higher conversion efficiency.

4. Conclusion

In this paper, the interactions among three laser waveforms and high-density plasma have been discussed. The simulation results have suggested that the asymmetric laser pulse waveform has a significant effect on the generation and energy absorption of fast electrons. The absorption efficiency of laser energy and the yield of fast electrons in the medium- and low-energy range can be efficiently improved by selecting a negative skew pulse (a laser waveform with a slow rising edge), which can lead to more efficient energy deposition in the fuel region. The above simulation results have been explained by comparing the plasma scale length at the front surface and the thickness of the absorption area. It has to be pointed out that in the case of the negative skew pulse, more high-energy fast electrons (> 5 MeV) have been inevitably generated as well, which needs to be avoided in the fast ignition scheme. This is a problem that needs further investigation in future studies.

Acknowledgement

This work was supported by the Strategic Priority Research Program of the Chinese Academy of Sciences (Nos. XDA25030100 and XDA25051000) and the National Natural Science Foundation of China (Nos. U1930107 and 11827807).

References

1. M. Tabak, J. Hammer, M. E. Glinsky, W. L. Kruer, S. C. Wilks, J. Woodworth, E. M. Campbell, M. D. Perry, and R. J. Mason, "Ignition and high gain with ultrapowerful lasers," Phys. Plasmas **1**, 1626 (1994).
2. J. Zhang, W. Wang, X. Yang, D. Wu, Y. Ma, J. Jiao, Z. Zhang, F. Wu, X. Yuan, Y. Li, and J. Zhu, "Double-cone ignition scheme for inertial confinement fusion," Phil. Trans. R. Soc. A **378**, 20200015 (2020).
3. T. Johzaki, Y. Nakao, and K. Mima, "Fokker–Planck simulations for core heating in subignition cone-guiding fast ignition targets," Phys. Plasmas **16**, 062706 (2009).
4. T. Yokota, Y. Nakao, T. Johzaki, and K. Mima, "Two-dimensional relativistic Fokker-Planck model for core plasma heating in fast ignition targets," Phys. Plasmas **13**, 022702 (2006).
5. M. Hata, H. Sakagami, A. Sunahara, T. Johzaki, and H. Nagatomo, "Effects of CH foam preplasma on fast ignition," Laser Part. Beams **30**, 189 (2012).
6. T. Nakamura, H. Sakagami, T. Johzaki, H. Nagatomo, K. Mima, and J. Koga, "Optimization of cone target geometry for fast ignition," Phys. Plasmas **14**, 103105 (2007).
7. T. Johzaki, H. Nagatomo, A. Sunahara, H. Cai, H. Sakagami, Y. Nakao, and K. Mima, "Pre-plasma effects on core heating and enhancing heating efficiency by extended double cone for FIREX," Nucl. Fusion **51**, 073022 (2011).
8. W. Theobald, A. A. Solodov, C. Stoeckl, K. S. Anderson, F. N. Beg, R. Epstein, G. Fiksel, E. M. Giraldez, V. Y. Glebov, H. Habara, S. Ivancic, L. C. Jarrott, F. J. Marshall, G. McKiernan, H. S. McLean, C. Mileham, P. M. Nilson, P. K. Patel, F. Pérez, T. C. Sangster, J. J. Santos, H. Sawada, A. Shvydky, R. B. Stephens, and M. S. Wei, "Time-resolved compression of a capsule with a cone to high density for fast-ignition laser fusion," Nat. Commun. **5**, 5785 (2014).
9. R. Kodama, H. Shiraga, K. Shigemori, Y. Toyama, S. Fujioka, H. Azechi, H. Fujita, H. Habara, T. Hall, Y. Izawa, T. Jitsuno, Y. Kitagawa, K. M. Krushelnick, K. L. Lancaster, K. Mima, K. Nagai, M. Nakai, H. Nishimura, T. Norimatsu, P. A. Norreys, S. Sakabe, K. A. Tanaka, A. Youssef, M. Zepf, and T. Yamanaka, "Fast heating scalable to laser fusion ignition," Nature **418**, 933 (2002).
10. H. Cai, S. Zhu, and X. He, "Effects of the imposed magnetic field on the production and transport of relativistic electron beams," Phys. Plasmas **20**, 072701 (2013).
11. M. Hata, H. Sakagami, T. Johzaki, and H. Nagatomo, "Effects of laser profiles on fast electron generation under the same laser energy," Laser Part. Beams **31**, 371 (2013).

12. J. Zhang, L. Chen, Y. Li, H. Teng, T. Lang, Z. Sheng, Q. Dong, L. Zhao, Z. Wei, and X. Tang, "Effect of laser polarization on the injection direction of superheated electrons in femtosecond laser plasma," Prog. Nat. Sci. **13**, 533 (2003).
13. T. Nakamura, H. Nagatomo, T. Johzaki, H. Sakagami, and K. Mima, "Numerical study on optimization of cone target and ignition pulse shape for fast ignition," J. Phys. **112**, 022049 (2008).
14. S. Kojima, Y. Arikawa, A. Morace, M. Hata, H. Nagatomo, T. Ozaki, S. Sakata, S. H. Lee, K. Matsuo, K. F. F. Law, S. Tosaki, A. Yogo, T. Johzaki, A. Sunahara, H. Sakagami, M. Nakai, H. Nishimura, H. Shiraga, S. Fujioka, and H. Azechi, "Energy distribution of fast electrons accelerated by high intensity laser pulse depending on laser pulse duration," J. Phys. **717**, 012102 (2016).
15. S. A. Ghasemi, M. Pishdast, and J. A. Yazdanpanah, "Numerical investigation of plasma heating during the entrance of an intense short laser pulse into a density profile," Laser Phys. **30**, 016001 (2020).
16. G. Zhang, D. Zou, Y. Ma, H. Zhou, F. Shao, X. Yang, Z. Ge, Y. Yin, T. Yu, C. Tian, L. Gan, J. Ouyang, and N. Zhao, "Effects of pulse temporal profile on electron bow-wave injection of electrons in laser-driven bubble acceleration," Acta Phys. Sin. **62**, 205203 (2013).
17. A. K. Upadhyay, S. A. Samant, and S. Krishnagopal, "Role of the laser pulse-length in producing high-quality electron beams in a homogenous plasma," Phys. Plasmas **19**, 073110 (2012).
18. Y. Huang, "Simulation research on chirped laser plasma electron acceleration," M.S. dissertation (Northeast Petroleum University, 2016).
19. M. Bake, B. Xie, S. Dulat, and A. Aimidula, "Electron acceleration in wake-field and supra-bubble regimes by ultraintense laser with asymmetric pulse," Commum. Theor. Phys. **55**, 883 (2011).
20. H. K. Malik and R. Gill, "Control of peaks of terahertz radiation and tuning of its frequency and intensity," Phys. Lett. A **382**, 2715 (2018).
21. D. K. Kuri, "Role of laser pulse asymmetry in electron acceleration in vacuum in the presence of an axial magnetic field," Phys. Plasmas **27**, 123102 (2020).
22. Y. Yao, C. Lu, S. Xu, J. Ding, T. Jia, S. Zhang, and Z. Sun, "Femtosecond pulse shaping technology and its applications," Acta Phys. Sin. **63**, 184201 (2014).
23. H. Zou and C. Zhou, "Femtosecond pulse shaping with space-time conversion technique," Laser Optoelectron. Prog. **42**, 2 (2005).
24. S. Chen, "Study on femtosecond laser pulses shaping and measurement technology," Ph.D. dissertation (Tianjin University, 2007).
25. L. Ji, B. Shen, X. Zhang, F. Wang, Z. Jin, C. Xia, M. Wen, W. Wang, J. Xu, and M. Yu, "Generating quasi-single-cycle relativistic laser pulses by laser-foil interaction," Phys. Rev. Lett. **103**, 215005 (2009).
26. M. S. Hur, Y. K. Kim, V. V. Kulagin, I. Nam, and H. Suk, "Versatile shaping of a relativistic laser pulse from a nonuniform overdense plasma," Phys. Plasmas **19**, 073114 (2012).
27. T. D. Arber, K. Bennett, C. S. Brady, D. A. Lawrence, M. G. Ramsay, N. J. Sircombe, P. Gillies, R. G. Evans, H. Schmitz, A. R. Bell, and C. P. Ridgers, "Contemporary particle-in-cell approach to laser-plasma modelling," Plasma Phys. Control. Fusion **57**, 113001 (2015).
28. X. Liu, S. Liu, and X. Yang, "Strong Langmuir turbulence excited by laser near critical surface," Laser Technol. **31**, 213 (2007).
29. F. Brunel, "Not-so-resonant, resonant absorption," Phys. Rev. Lett. **59**, 52 (1987).
30. D. W. Forslund, J. M. Kindel, and K. Lee, "Theory of hot-electron spectra at high laser intensity," Phys. Rev. Lett. **39**, 284 (1977).
31. W. L. Kruer and K. Estabrook, "J×B heating by very intense laser light," Phys. Fluids **28**, 430 (1985).
32. S. C. Wilks, "Simulations of ultraintense laser–plasma interactions," Phys. Fluids B **5**, 2603 (1993).
33. H. Cai, K. Mima, A. Sunahara, T. Johzaki, H. Nagatomo, S. Zhu, and X. He, "Prepulse effects on the generation of high energy electrons in fast ignition scheme," Phys. Plasmas **17**, 023106 (2010).
34. E. Lefebvre and G. Bonnaud, "Nonlinear electron heating in ultrahigh-intensity-laser–plasma interaction," Phys. Rev. E **55**, 1011 (1997).
35. W. Yu, V. Bychenkov, Y. Sentoku, M. Yu, Z. Sheng, and K. Mima, "Electron acceleration by a short relativistic laser pulse at the front of solid targets," Phys. Rev. Lett. **85**, 570 (2000).